JOURNAL OF OPTOELECTRONICS AND ADVANCED MATERIALS Vol. 9, No. 5, May 2007, p. 1198 - 1205

Plenary Lecture

Challenges in growth of high-performance scintillator crystals

DIRK EHRENTRAUT, AKIRA YOSHIKAWA, TSUGUO FUKUDA*
Institute of Multidisciplinary Research for Advanced Materials, Tohoku University, 2-1-1 Katahira, Aoba-ku, Sendai 980-8577, Japan

Inorganic scintillator crystals are in steadily growing demand. High purity controlled doping and structural perfection of scintillator crystals is inevitable, what certainly is challenging the growth technology. We review our recent progress in the fabrication and characterization of scintillator crystals like 8 inches size BaF_2 (super fast decay of about 600 ps), Pr^{3+} doped $Lu_3Al_5O_{12}$ and $Y_3Al_5O_{12}$ (high light yields) and undoped and In^{3+} doped ZnO. The latter shows two-component super fast decay (fast component 30-60 ps, slow component 250-800 ps). GaN might be the next candidate crystal to show fast luminescence, once good crystal quality is available.

(Received November 14, 2006; accepted April 12, 2007)

Keywords: Scintillator crystal, BaF_2, $Lu_3Al_5O_{12}$, In^{3+} doped ZnO, GaN

1. Introduction

Radiation detection by scintillators is widely used in industry, health care and scientific research [1,2]. Applications include X-ray computer tomography (CT), positron emission tomography (PET), time-of-flight (TOF)-PET for higher special resolution, or high energy and nuclear particle physics to name a few.

Basically, a scintillator transforms high-energy photons into photons in the ultra violet (UV) or visible light (VIS) spectral region, which can easily and with high sensitivity be detected by conventional detectors such like photomultiplier. Material requirements depend on the particular application and include high integral efficiency, high light yield and energy resolution, suitable emission wavelength, speed of scintillation response (luminescence decay and transport processes), density, radiation hardness and price of fabrication. Latter feature is of interest when it comes to industrial production.

Scintillator crystals can be comprised as a special class of crystals fulfilling above criteria and are characterized by high crystallinity at very low impurity concentration. This is particularly important to reduce efficiency-lowering traps. Also, doping is often applied to improve light yield.

Fig. 1 comparatively shows the decay time over light yield for a range of known scintillator crystals and gives the outlook what is next required from scintillators. Next generation scintillators involve both features: fast decay and high light yield. Among the most promising candidate materials right now are ZnO, BaF_2 and Pr doped $Lu_3Al_5O_{12}$ (LuAG).

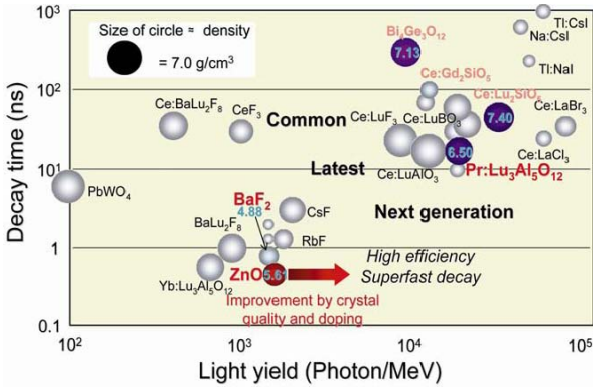

Fig. 1. Overview over important scintillator crystals in terms of decay time versus light yield. The size of the circle relates to the density of the material.

It is easy to understand that crystal growth technology plays a crucial role in order to meet the needs for a scintillator crystal. This paper has the focus on recent developments in crystal growth of large BaF_2, Pr^{3+} doped oxides, undoped and In^{3+} doped ZnO and GaN, which was achieved in our laboratory [3-6]. As different as the crystals are so are the growth technologies we have to employ. Micro pulling down (μ-PD) method serves for the fast-screening of melt grown crystals like BaF_2 and Pr doped LuAG and $Y_3Al_5O_{12}$ (YAG). Promising growth conditions would have been transferred to the Czochralski (Cz) growth technique, which allows the fabrication of large-size crystals but is more time-consuming than μ-PD. ZnO and GaN require the growth from solution as they are

decomposing under normal pressure instead of congruently melting. Therefore, we apply the hydrothermal and ammonothermal growth under elevated temperatures (300-550°C) and pressures (≤ 150 MPa). Since both solvothermal techniques can only realize slow growth rates and doping is an unsolved issue as well, a route towards ZnO thin film growth by liquid phase epitaxy (LPE) was developed in our group [6]. This technology is being used as fast-screening tool for doped ZnO, likewise the μ-PD method for congruently melting crystals.

2. BaF_2

Barium fluoride (BaF_2, fluorite structure, ρ = 4.89 g cm^{-3}) is very appealing for TOF-PET devices in spite of its super fast scintillation response in the cross-luminescence component (τ = 0.6 ns) and rather intense (1400 photons/MeV) UV scintillation component at λ = 220 nm [7,8]. Disadvantageously is the relatively low density of BaF_2 (ρ = 4.89 g cm^{-3}), thus providing moderate stopping power only.

Low thermal conductivity and pronounced cleavage challenges the crystal growth. Both Bridgman (BM) and Czochralski (CZ) method can be employed. Although the simple equipment speaks for BM, serious distortion of the crystal derived from the crucible wall restrains, moreover, crystal orientation is limited. We therefore have chosen the CZ method to obtain best-possible crystallinity and homogeneity.

For the first time, recently we published [3] on the growth of 8 inch diameter BaF_2 grown on $\langle 111 \rangle$ seeds from high-purity carbon crucible by the CZ method under oxygen-free argon (Ar, 99.9999%) atmosphere. Prior to filling the recipient with Ar, vacuum conditions of 10^{-4} Pa were used while heating up to 300°C to remove absorbents from inner part of the recipient. Essential is the addition of 1 wt% PbF_2 to the BaF_2 melt acting as scavenger to bind remaining oxygen. Control of temperature distribution is a critical issue, which has been conducted by means of 3 heaters and adequate thermal insulation setup, see ref. 3 for detailed experimental setup. To test our growth setups, firstly we have been grown CaF_2 as a model crystal for BaF_2. Fig. 2 compares the quality of polished slices of our CZ-grown CaF_2 and BaF_2, which are both completely transparent, colorless crystal and free of any visible scatters. The BaF_2 crystal was grown at the pulling rate of 3-5 mm/h along with 4 rpm clockwise seed rotation and 1 rpm counter clockwise crucible rotation was applied. Noteworthy is the large opening angle of the shoulder region of the crystal, see insert in Fig. 2a, to quickly gain the final crystal diameter of 200 mm. Growth time and material losses are significantly reduced such way.

a

b

Fig. 2. Cross sectional view down the optical-grade-polished 8 inch crystal sliced of (a) CaF_2 and (b) BaF_2. Insert in (b) shows the crystal before cutting.

Fig. 3 shows the optical band edge around 140 nm. About 80% transmittance is seen at wavelengths ≥ 200 nm for the 2 mm thick sample.

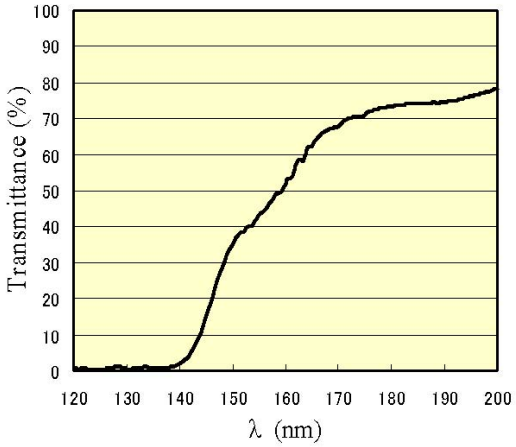

Fig. 3. Transmission spectrum of BaF_2.

Fig. 4 displays the absorption of BaF_2 after X-ray (25 kV, 180 mA) irradiation at the dose of 240 Gy at RT for 30 minutes. Two peaks around 230 and 290 nm are induced of which the highest energy absorption band was

ascribed to the simple F center [3]. It should be noted here that radiation hardness still has to be improved.

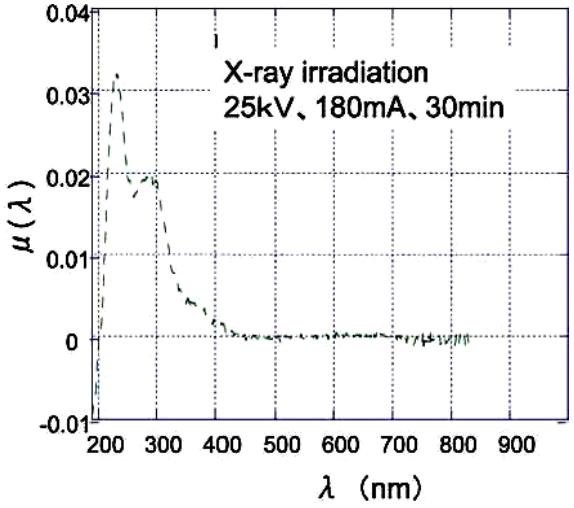

Fig. 4. Absorption spectrum of BaF_2 upon X-ray irradiation.

Fig. 5 shows the photoluminescence (PL) decay at room temperature (RT) upon laser pulse excitation (λ = 290 nm). A streak camera was used for recording the signal. A single exponential fitting derives the decay time $\tau \leq 0.63$ ns, which is very well in accordance with the literature [7,8]. However, we have shown that feature for a large crystal for the first time.

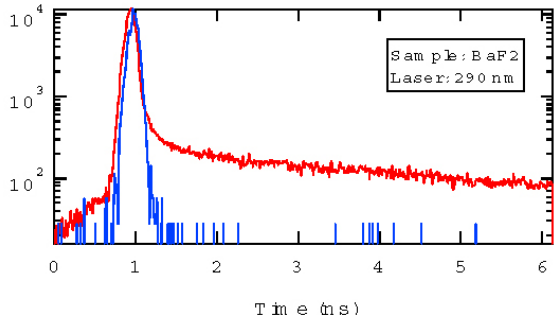

Fig. 5. Photoluminescence decay of BaF_2 upon laser excitation at 220 nm at room temperature.

3. Praseodymium doped $Lu_3Al_5O_{12}$ and $Y_3Al_5O_{12}$

Scintillators with the presently best figure-of-merit (combination of stopping power, speed of scintillation response and light yield) are Ce-activated materials [2]. However, there is continuous need to further improve the performance of materials. We therefore explored the Pr^{3+} ion, which shows similar 5d-4f transition in wide band gap materials having medium/high crystal field strength like Ce^{3+}, but is comparatively less studied.

As host crystal, particularly the $Lu_3Al_5O_{12}$ (LuAG) provides a high density of ρ = 6.7 g cm^{-3}, and growth and machining of both garnet-type materials LuAG and $Y_3Al_5O_{12}$ (YAG, ρ = 4.55 g cm^{-3}) is well established. The growth of high-quality YAG crystal is easier to achieve and was therefore chosen to test incorporation and effects of the Pr^{3+}.

Pr doped LuAG and YAG single crystals were grown (μ-PD, Cz) with different doping levels up to 3 mol% Pr [4,9]. Typical pulling rates in case of μ-PD were 0.05-0.2 mm min^{-1} at crystal diameter 5 mm and Cz growth yields best results at 1.2 mm h^{-1} at rotation rate of 15 rpm. The seed was oriented towards $\langle 111 \rangle$. Further conditions of the Cz growth include the use of an Ir crucible, N_2 atmosphere and usage of a software code to enable computerized automatic diameter control, see refs. 4,9. The growth by μ-PD method is detailed in ref. 10. Fig. 6 depicts a 1%Pr doped LuAG crystal grown by the Cz technique. This doping level is already high. The crystal is completely transparent, slightly pale green in appearance and crack-free.

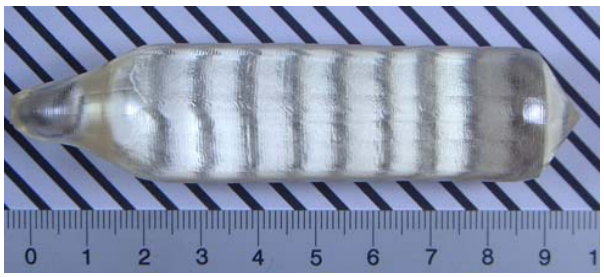

Fig. 6. A 1% Pr-doped LuAG crystal by Czochralski technique.

A difficulty is the small effective distribution coefficient k_{eff} = 0.06 for Cz-grown crystals due to the comparatively larger ionic radius of the Pr^{3+} than the Lu^{3+}. This may limit the concentration of Pr^{3+} in the crystal.

Plates of 1 mm in thickness were prepared for spectroscopic measurement. Radioluminescence (RL) spectra and PL decays were studied from 80-450 K using a Spectrofluorometer 199S equipped with UV (steady state and ns coaxial H_2 flash lamp) and X-ray (steady state tube, 35 kV, Mo) excitation sources. Scintillation light yield and energy resolution were determined from energy spectra obtained under 611 keV γ-ray excitation by ^{137}Cs source and detection by a Hamamatsu H6521 photomultiplier.

In Fig. 7 is shown the absorption of 0.25% Pr doped LuAG and YAG. The absorption bands at 240 and 285 nm can be ascribed to the two lowest 4f($^3H_4$)→5d$_{1,2}$ transition of the Pr^{3+}, respectively. The weak 4f-4f absorption between 400-600 nm is seen in the insert of the figure.

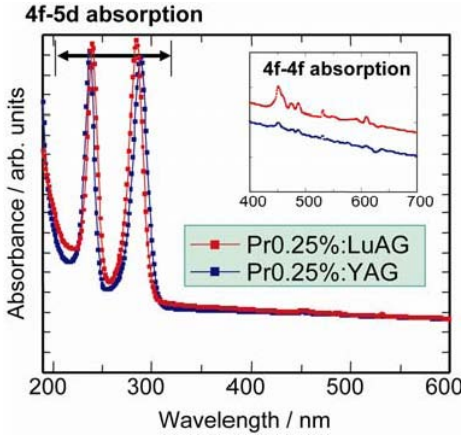

Fig. 7. Absorption of 0.25% Pr-doped YAG and LuAG shows characteristic peaks due to 4f-5d absorption.

Fig. 8 shows the emission spectra of 0.25% Pr doped LuAG and YAG upon excitation of the absorption bands (Fig. 7) with 280 nm. Structured emission is seen in both samples. The Pr doped LuAG appears with a dominant peak at 306 nm, which is slightly high-energy shifted with respect to that of Pr doped YAG and can be ascribed to radiative transition from the 5d state to ^3H_x and ^3F_x states of the 4f states [11]. The intensity from this transition in Pr doped LuAG sample is two times higher than that of Pr doped YAG. By contrast, the 4f-4f transition in Pr doped YAG is higher than for Pr doped LuAG.

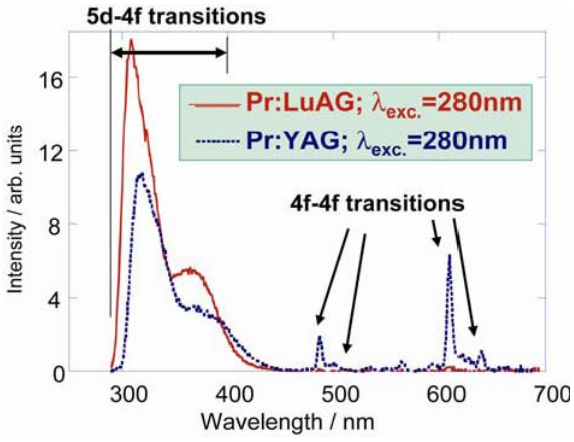

Fig. 8. Emission at 310 and 370 nm due to 5d-4f transition.

Room temperature PL decay for emission at 310 nm is shown in Fig. 9. Emission decay of Pr doped YAG (Fig. 9a) was 12ns and that of Pr doped LuAG (Fig. 9b) was 17ns. No difference was observed for the decay time of the 310 and 370 nm emission. Spectrally unresolved scintillation decay (see ref. 9 for details) shows a dominant component about 20 ns, which is much shorter than for Lu_2SiO_5 (40 ns) or $Bi_4Ge_3O_{12}$ (BGO, 300 ns), see also Fig. 1. Along with observed slower decay components about 450 ns, re-trapping processes and delayed radiative recombination at Pr^{3+} emission centers were pointed out to be the reason [9].

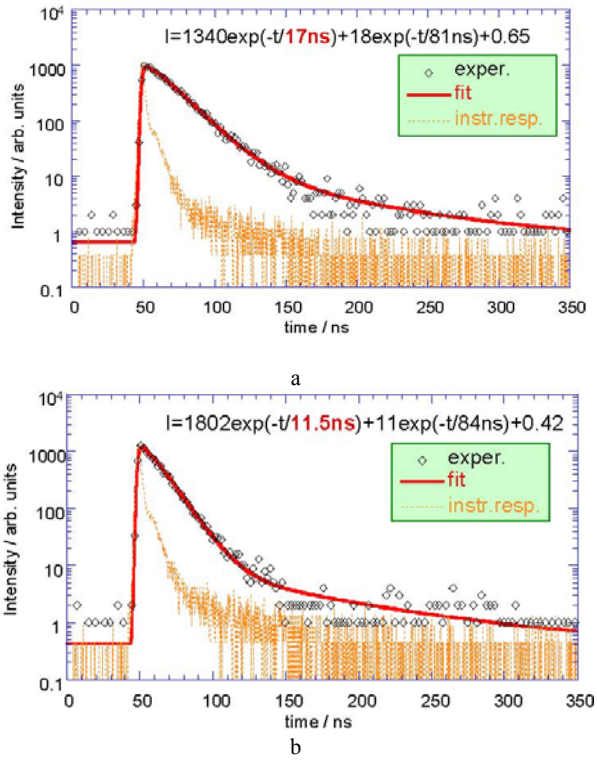

Fig. 9. Room temperature photoluminescence decay of 0.25% Pr doped (a) YAG and (b) LuAG crystal upon excitation at 280 nm.

The relative scintillation light yield was highest for 0.2-0.3% Pr doped LuAG and is 2-3 times greater than the BGO standard sample [9].

4. ZnO bulk and film

The wurtzite-type zinc oxide (ZnO, ρ = 5.61 g cm^{-3}) is a direct wide band gap (3.4 eV) semiconductor. An intrinsic problem in ZnO is the high re-absorption losses due to the small Stokes shift of Wannier exciton-based emission. Later effect can be easily responsible for relatively low luminescent intensity from bulk samples under the high-energy excitation. Fig. 10 shows the RL and absorption spectra as recorded from an undoped ZnO crystal at 80 K and room temperature (RT). While at 80 K at least the longitudinal optical (LO) phonon replica of the exciton emission is still out of the absorption edge of a 1 mm thick plate, a much larger part is getting absorbed at RT. The possible way to overcome the dilemma could be to red-shift the generated emission, away from the intrinsic absorption edge at about 390 nm at 295 K. Therefore, the doping with donors like In^{3+} was tried.

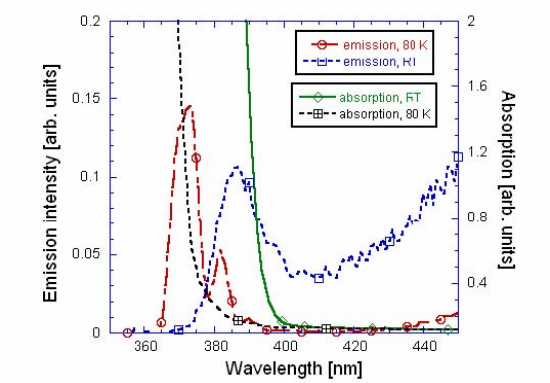

Fig. 10. Radioluminescence and absorption of a 1 mm thick ZnO sample at 80 K and room temperature around the band edge.

Recently, ultra fast scintillation decay in the sub-nanosecond range was reported for the Ga-doped ZnO powder at RT upon exposure to pulsed X-ray light (35 ps, 18 keV [12]) Moreover, In^{3+} doped ZnO single crystal showed super fast scintillation response time of 0.65 ns [13], apparently limited by instrumental response.

Together with an industrial partner our laboratory is strongly involved in the technology development for the hydrothermal growth of large size ZnO crystals. This resulted in the growth of 2 inch size (0001) crystals [5]. Fig. 11 displays a batch of crystals grown during one process run. We employed autoclaves with Pt inner container to prevent from corrosion and impurity incorporation into the growing crystal. Best mineralizer molar combination to increase the solubility of ZnO in the supercritical water was 1 LiOH/3 KOH. Lithium is inevitable to suppress formation of crystal defects. Consequently, traces of Li and K would be found in the crystal. By inductively coupled plasma mass spectrometry (ICP-MS) we detected < 12 ppm Li, < 0.3 ppm K, < 1 ppm Fe, and < 0.5 ppm Al in wafers prepared from the crystal fraction grown in the $\langle 0001 \rangle$ direction [5].

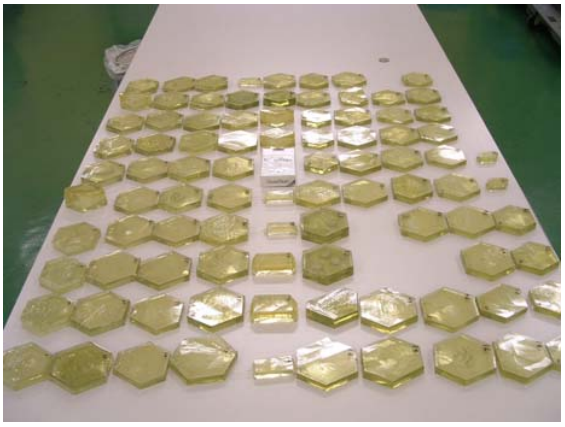

Fig 11. ZnO crystals of 2 inch size from a single growth run.

The doping of ZnO with In^{3+} during hydrothermal bulk crystal growth appears to be quite troublesome and only small (3 mm and <0.2 mm thickness) size crystals were yielded upon parasitic nucleation. We therefore used our recently developed LPE technology [6] to produce undamaged surfaces of In^{3+} doped ZnO. Mechanically untouched ZnO surfaces are desirable to exclude radiative losses due to a damaged surface layer [6]. By PL and RL measurements a chemical-mechanically polished (CMP) ZnO substrate was compared to an undoped ZnO film fabricated by LPE on before mentioned ZnO substrate. The excitonic emission from the CMP ZnO substrate almost vanished at RT to the favor of a defect-based broad emission band in the visible spectral region. By contrast, the excitonic emission is clearly visible from the mechanically untouched epitaxial ZnO film. A clear picture of sharp peaks from both free and donor-bound exciton due to the damage-free surface was observed.

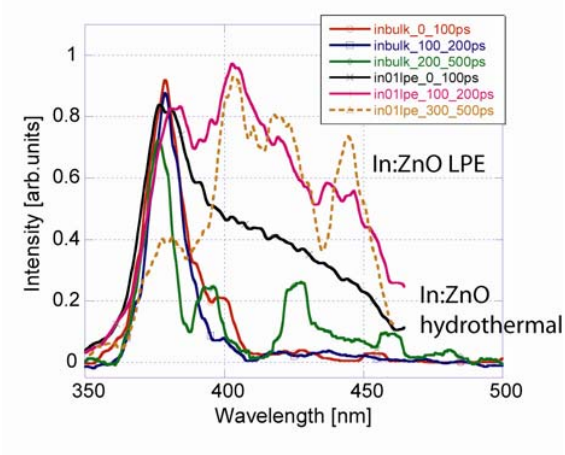

FIig. 12. Time-resolved luminescence of the In^{3+} doped hydrothermal ZnO sample and In^{3+}, Li^{+} co-doped (0001) homoepitaxial ZnO film.

The growth of ZnO films by LPE obtains very high crystal perfection and dopant incorporation in a controlled fashion is possible within thermodynamic limitations of solubility [14]. ZnO films were grown at a constant temperature of 640°C under air atmosphere and pressure. The growth solution contains LiCl, $ZnCl_2$ and K_2CO_3 in purities of ≥99.99%. Best film qualities have been fabricated from the ZnO concentration of 13 mmol per mol LiCl. Details on film preparation are given elsewhere [6,14]. Doping with In^{3+} is enabled through employment of 99.99% $InCl_3$. The substrate was hydrothermally grown ZnO with a surface finish produced by chemical-mechanical polishing and followed by thermal annealing (1100 °C, 4 h, oxygen). Atomic steps (step spacing ≈150 μm) are typically found by atomic force microscopy. Controlled 2-dimensional nucleation and film growth was therefore achieved and the undoped films grew accordingly to the step-flow mode [6]. Doping by In^{3+}, however, is influential on the growth mode, exhibited by changes in the surface morphology of a film. The insert of

Fig. 13 shows the In^{3+}, Li^{+} co-doped ZnO film of the thickness of 1 μm as observed by differential interference microscopy. Lithium is incorporated from the solvent at levels about 10^{18}-10^{19} atoms cm^{-3} and the In concentration is typically higher by at least one order of magnitude as derived by secondary ion mass spectrometry (SIMS). The film we discuss here contains 6×10^{19} In atoms cm^{-3} (about 0.1 mol% In).

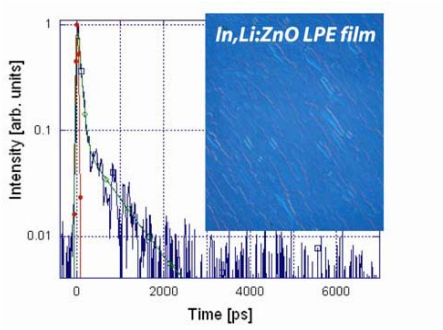

Fig. 13 Room temperature photoluminescence decay from the In, Li co-doped ZnO film upon excitation by a 150-fs laser pulse at 260 nm. , λ_{em} = 380-390 nm, RT. Solid line is convolution of the instrumental response with the two-exponential approximation of the decay curve. The insert is a micrograph of the In^{3+},Li^{+} co-doped (0001) homoepitaxial ZnO film taken by differential interference microscopy.

The XRC crystallinity (ATX-E Rigaku diffractometer, $CuK_{\alpha 1}$, four crystal Ge (220) channel monochromator, beam divergence 12 arcsec, scan speed 0.01° min^{-1}, step width 10^{-4} °) employing the (0002) reflection of the specimen in Fig. 13 is ≤ 35 arcsec what is very close to that of ZnO bulk suggesting low residual strain in the film. The In-doped film exhibits well-aligned steps parallel to the $(10\bar{1}0)$ facet with step spacing of 5-10 μm.

Fig. 14. A transparent GaN crystal as grown by the acidic ammonothermal technique.

Time-resolved luminescence of the In^{3+} doped hydrothermal ZnO sample and In^{3+}, Li^{+} co-doped (0001) homoepitaxial ZnO film is shown in Fig. 12. Upon excitation by femtosecond laser pulse (Ti-sapphire laser, 150 fs pulse at λ_{exc} = 260 nm; Clark-MXR CPA2001) luminescence data were recorded using polychromator and a 2-dimensional CCD sensor at the output of a streak camera (Hamamatsu C2830), which allow simultaneous evaluation of time-resolved spectra (TRS) and luminescence decays. In a recent paper [15] TRS was discussed for the In doped films and the bulk crystal. RT time-resolved spectra (TRS) from In-doped films for the time-window of 0-100 ps yielded considerable emission intensity from 400-420 nm (Fig. 12). This emission becomes clearly prevalent for the time-window 300-500 ps and is ascribed to the donor-acceptor pair (DAP) recombination as our LPE films contain a considerable amount of Li derived from the growth solution [15]. By contrast, there is no such effect for the In doped hydrothermally grown ZnO, which does contain smaller amount of Li than the LPE sample. The peak around 430 nm for 200-500 ns accumulation time is likely related to some defects.

Considering the value of the band gap of ZnO, the binding energy of In^{3+} donor ions of about 50 meV, the binding energy of the Li acceptor between 300-500 meV [16,17] and further effect of Coulombic interaction depending on the donor-acceptor distance, the position of the expected emission band is just round 400-420 nm in good agreement with the observed emission spectrum of the In-doped film at longer times [15].

PL decay of the In^{3+}, Li^{+} co-doped ZnO film upon the fs laser excitation is shown in Fig. 13. The wavelength region of 380-390 nm was extracted. The decay follows a two-exponential course. The faster component shows typically 30-60 ps decay time, while the slower component one ranges 250-800 ps. Intensity of the latter component was increasing towards longer emission wavelengths. The interpretation of the luminescence decay in the LPE films was not straightforward. Decay times can easily scale down to 100 ps or less in case that any kind of bound excitons would contribute to the emission process [18]. The slower decay component above 400 nm in the In^{3+}, Li^{+} co-doped film is apparently related to the decay kinetics of the DAP recombination and point to very fast character of this process as well. In the case of such pair radiative recombination process, rather non-exponential decay is expected, however.

Such a fast sub-nanosecond emission process based on donor-acceptor recombination could be well exploited for scintillator application as it is sufficiently shifted from the ZnO absorption edge. Re-absorption losses are thus minimized. The timing characteristics obtained for the In^{3+},Li^{+} co-doped ZnO film are clearly superior with respect to those obtained at $(n\text{-}C_6H_{13}NH_3)_2PbI_4$, a natural thin film-multiple quantum well structure, which was recently announced as a material of choice to obtain super fast scintillation time response [19].

5. GaN

Like ZnO, wurtzite-type GaN (ρ = 6.1 g cm^{-3}) might be of interest as semiconducting scintillator due to its similar electronic structure (direct band gap, excitonic

emission around 3.4 eV). However, large and high-quality crystals are no yet available.

We employ the ammonothermal growth technique, which is very similar to the hydrothermal growth of quartz and ZnO [20,21]. Detailed procedure on experimental conditions has been published recently [22]. Supercritical ammonia (NH_3) serves as solvent and solubility-enhancing acidic mineralizer like NH_4Cl are utilized. The feedstock for GaN is either Ga metal or GaN. This growth environment provides a regular solubility, i.e. GaN is deposited on the GaN seed crystal upon controlled temperature decrease. Like for ZnO, we work with Pt inner liner to prevent the autoclave from corrosion.

Fig. 13 provides a transparent and crack-free GaN crystal which was grown on the (0001) HVPE-grown GaN seed. The thickness of the grown crystal oversteps 0.2 mm for the growth duration of 10 days. The feedstock was a mixture of Ga metal and polycrystalline GaN. Crystallinity has been measured with XRC and epitaxial relationship with the seed was evidenced. The XRC FWHM from (0002) reflection is about 0.3 to 0.5°. This points to the fact that still much work has been left to improve nucleation behavior and control of the growth parameters mass transport (from feedstock to the crystal), temperature uniformity in the growth zone and optimum temperature program.

First PL and RL measurements will soon be started with better GaN crystals. If successful, there is quite some potential to combine in a single device the scintillator properties of GaN with the already well-developed III-nitride electronics.

6. Conclusions

We gave an overview on our recent achievements in the growth and characterization of scintillator crystals with extraordinary luminescent features. BaF_2 is characterized by a fast cross-luminescence component (τ = 0.6 ns) and intense UV scintillation at λ = 220 nm. It can be grown with high structural perfection up to 8 inch in size by the Cz method. Pr doped $Lu_3Al_5O_{12}$ shows a fast decay component of 12 ns at 310 nm emission wavelength. The light yield is 2-3 times larger than for the BGO standard. A broad emission in the 400-420 nm spectral regions of In^{3+},Li^+ co-doped LPE films was obtained at room temperature, and is ascribed to the donor-acceptor pair recombination enabled by high content of Li^+ ions in the films. Characteristic is a two-component luminescence decay with a fast component of τ = 30-60 ps and a slower one of τ = 250-800 ps. The luminescence properties of bulk GaN will be exploited in near future upon availability of crystals. The ammonothermal growth technique may provide suitable material.

Acknowledgements

This work was partially supported by Special Coordination Funds of the Ministry of Education, Culture, Sports, Science and Technology of the Japanese government (MEXT), Innovation Plaza Miyagi project from the Japan Science and Technology Agency (JST), the Industrial Technology Research Grant Program in 03A26014a from the New Energy and Industrial Technology Development Organization (NEDO) and a Grant in Aid for Young Scientists (A), 15686001, 2003 from MEXT.

References

[1] M. Nikl, Meas. Sci. Technol., 2006, **17**, R37-R54.
[2] K. W. Krämer, P. Dorenbos, H. U. Güdel, C. W. E. Van Eijk, J. Mater. Chem. **16**, 2773 (2006).
[3] K. Kamada, T. Nawata, Y. Inui, H. Yanagi, H. Sato, A. Yoshikawa, M. Nikl, T. Fukuda, Nucl. Instrum. Methods Phys. Res. A **537,** 159 (2005).
[4] H. Ogino, A. Yoshikawa, M. Nikl, A. Krasnikov, K. Kamada, T. Fukuda, J. Cryst. Growth **287**, 335 (2006).
[5] E. Ohshima, H. Ogino, I. Niikura, K. Maeda, M. Sato, M. Ito, T. Fukuda, J. Cryst. Growth **260,** 166 (2004).
[6] D. Ehrentraut, H. Sato, M. Miyamoto, T. Fukuda, M. Nikl, K. Maeda, I. Niikura, J. Cryst. Growth **287,** 367 (2006).
[7] M. Laval, Nucl. Instrum. Methods Phys. Res. A **206,** 169 (1983).
[8] P.A. Rodnyi, M. A. Terekhin, E. N. Mel'chakov, J. Lumin. **47**, 281 (1991).
[9] H. Ogino, A. Yoshikawa, M. Nikl, K. Kamada, T. Fukuda, J. Cryst. Growth, 2006, DOI: 10.1016/j.jcrysgro.2006.04.021.
[10] T. Fukuda, P. Rudolph, S. Uda (Eds.), Fiber Crystal Growth from the Melt, 2004, Springer Verlag, Berlin.
[11] M. Nikl, H. Ogino, A. Krasnikov, A. Beitlerova, A. Yoshikawa, T. Fukuda, phys. stat. sol. a **202**, R4-R6 (2005).
[12] S. E. Derenzo, M. J. Weber, M. K. Klintenberg, Nucl. Instrum. Methods Phys. Res. A **486,** 214 (2002).
[13] P. J. Simpson, R. Tjossem, A. W. Hunt, K. G. Lynn, V. Munné, Nucl. Instrum. Methods Phys. Res. A **505,** 82 (2003).
[14] H. Sato, D. Ehrentraut, T. Fukuda, Jpn. J. Appl. Phys. **45,** 190 (2006).
[15] D. Ehrentraut, H. Sato, Y. Kagamitani, A. Yoshikawa, T. Fukuda, J. Pejchal, K. Polak, M. Nikl, H. Odaka, K. Hatanaka, H. Fukumura, J. Mater. Chem., 2006, DOI: 10.1039/b608023e.
[16] B. K. Meyer, J. Sann, A. Zeuner, Superlatt. Microstr. **38**, 344 (2005).
[17] B. K. Meyer, H. Alves, D. M. Hofmann, W. Kriegseis, D. Forster, F. Bertram, J. Christen, A. Hoffmann, M. Straβburg, M. Dworzak, U. Haboeck and A. V. Rodina, Phys. Status Solidi (b) **241,** 231 (2004).
[18] L. Fan, H. Song, L. Yu, Z. Liu, L. Yang, G. Pan, X. Bai, Y. Lei, T. Wang, Z. Zheng, X. Kong, Opt. Mater., 2006, doi:10.1016/l.optmat.2005.08.046.

[19] K. Shibuya, M. Koshimizu, H. Murakami, Y. Muroya, Y. Katsumura, K. Asai, Jpn. J. Appl. Phys. **43,** L1333 (2004).
[20] R. Dwiliński, J. Doradziński, J. Garczyński, L. Sierzputowski, J. M. Baranowski, M. Kamińska, Mater. Sci. Eng. **B50**, 46 (1997).
[21] A. Yoshikawa, E. Ohshima, T. Fukuda, H. Tsuji, K. Oshima, J. Cryst. Growth **260**, 67 (2004).
[22] Y. Kagamitani, D. Ehrentraut, A. Yoshikawa, N. Hoshino, T. Fukuda, S. Kawabata, K. Inaba, Jpn. J. Appl. Phys. **45**, 4018 (2006).

*Corresponding author: t-fukuda@tagen.tohoku.ac.jp